

**Robust hybridization gap in the Kondo insulator YbB<sub>12</sub> probed by femtosecond optical spectroscopy**A. R. Pokharel <sup>1</sup>, S. Y. Agustsson <sup>1</sup>, V. V. Kabanov <sup>2</sup>, F. Iga <sup>3</sup>, T. Takabatake <sup>4</sup>, H. Okamura <sup>5</sup> and J. Demsar <sup>1</sup><sup>1</sup>*Institute of Physics, Johannes Gutenberg-University Mainz, 51099 Mainz, Germany*<sup>2</sup>*Dept. of Complex Matter, Jozef Stefan Institute, 1000 Ljubljana, Slovenia*<sup>3</sup>*Institute for Quantum Beam Sciences, Ibaraki University, Mito 310-8512, Japan*<sup>4</sup>*Graduate School of Advanced Science and Engineering, Hiroshima University, Higashi-Hiroshima 739-8530, Japan*<sup>5</sup>*Graduate School of Technology, Industrial and Social Sciences, Tokushima University, Tokushima 770-8506, Japan*

(Received 24 November 2020; revised 4 March 2021; accepted 5 March 2021; published 18 March 2021)

In heavy fermions the relaxation dynamics of photoexcited carriers has been found to be governed by the low energy indirect gap  $E_g$  resulting from hybridization between localized moments and conduction band electrons. Here, carrier relaxation dynamics in a prototype Kondo insulator YbB<sub>12</sub> is studied over a large range of temperatures and over three orders of magnitude. We utilize the intrinsic nonlinearity of dynamics to quantitatively determine microscopic parameters, such as electron-hole recombination rate. The extracted value reveals that hybridization is accompanied by a strong charge transfer from localized  $4f$  levels. The results imply the presence of a hybridization gap up to temperatures of the order of  $E_g/k_B \approx 200$  K, which is extremely robust against electronic excitation. Finally, below 20 K the data reveal changes in the low energy electronic structure, attributed to short-range antiferromagnetic correlations between the localized levels.

DOI: [10.1103/PhysRevB.103.115134](https://doi.org/10.1103/PhysRevB.103.115134)**I. INTRODUCTION**

The interaction between multiple degrees of freedom giving rise to the exotic phases of matter is one of the most intriguing aspects of modern solid-state physics. Heavy fermion compounds with partially filled  $4f$ - or  $5f$ -electron shells present one of the most challenging material classes, hosting different electronic, magnetic, and thermodynamic phases at low temperatures ( $T$ ) [1–3]. At high  $T$ , localized  $f$  electrons are only weakly interacting with conduction ( $c$ ) electrons. As the temperature is lowered below the material specific Kondo temperature ( $T_K$ ), the localized moments, residing in the sea of conduction electrons, hybridize with them. This  $c$ - $f$  hybridization results in the formation of an (indirect) hybridization gap in the density of states (DOS) [1,4,5]. In metallic heavy fermion systems the Fermi level lies in one of the flat  $c$ - $f$  hybridized bands while in Kondo insulators Fermi level resides within the hybridization gap. Upon further cooling, intersite correlations of localized magnetic moments in a dense periodic Kondo lattice can give rise to a magnetic long range order. The exact  $T$  dependence of the low-energy electronic structure, which manifests itself, e.g., in a crossover between the small and large Fermi surface in heavy fermions [6,7] and in the  $T$  dependence of the electronic effective mass, as well as the underlying microscopic mechanisms have been the topic of intense research efforts in recent years [6–9].

In addition to photoemission spectroscopy (PES) [7,9] and tunneling spectroscopy [8], femtosecond real-time approaches have also been shown to be highly sensitive to changes in the low-energy electronic structure of heavy electron systems. Here, studies on a series of heavy fermions [10–17] as well as on the Kondo insulator SmB<sub>6</sub> [11,12,18] were

performed, demonstrating the relaxation of photoexcited carriers to be governed by the presence of the hybridization gap near the Fermi level [12]. The dramatic slowing down of carrier relaxation at low temperatures [10–15,17], in some cases by orders of magnitude [12], was qualitatively accounted for by the phenomenological model [12], originally developed to describe the relaxation dynamics in fully-gapped superconductors [19–23]. The model, given by the set of coupled nonlinear rate equations, describes the recombination of photoexcited electron-hole pairs across the indirect hybridization gap via emission of large-momentum, high-frequency phonons. The reabsorption of the latter eventually limits the relaxation process. In addition to time-resolved studies with near-infrared pulses [10–15,17], the dynamics of Kondo insulators was recently investigated also by time-resolved PES (tr-PES) [24] and transient THz spectroscopy [18], providing direct spectroscopic support to the above scenario. While there is mounting evidence supporting the above description, the nonlinear nature of the relaxation processes should enable quantifying the underlying microscopic parameters and provide details on the nature of the  $c$ - $f$  hybridization. For such a quantitative characterization, a well studied prototypical Kondo insulator should be used.

YbB<sub>12</sub> is one of the most studied Kondo insulators [24–28] that recently regained interest also as a candidate for hosting a nontrivial topological surface state [29–32]. Optical data reveal a fully open indirect hybridization gap of  $E_g \sim 20$  meV below  $\sim 25$  K, with a crossover to the metallic behavior near  $\sim 80$  K [25]. Similar values of  $E_g$  at low  $T$  were extracted also from the high resolution PES [26,27], while transport measurements suggest  $E_g \sim 13$  meV [28]. Interestingly, a combined PES and tr-PES study suggests the gap closing

above  $T \approx 100$  K [24]. Thus, while the existence of a gap at low  $T$  is unambiguous, its  $T$  dependence and robustness against external stimuli has yet to be clarified.

In this paper, we explore in detail the temperature and excitation density dependence of carrier relaxation dynamics in one of the best-known Kondo insulators  $\text{YbB}_{12}$ . We demonstrate that the (nonlinear) dynamics over a large range of temperatures and over three orders of magnitude in excitation density can be quantitatively described by the relaxation bottleneck model [11,12]. Quantitative analysis provides access to the microscopic electron-hole recombination rate  $R$ , which is found to be about three orders of magnitude lower than in superconductors with comparable gap energy [21–23]. We ascribe this observation to an enhanced density of states, which is a result of the charge transfer from localized  $4f$  states that is accompanying hybridization. We show that the indirect hybridization gap,  $E_g \sim 15$  meV, persists near the room temperature and is extremely robust against electronic excitation, up to the absorbed energy densities of  $\approx 140$  meV per unit cell volume (ucv). Finally, for  $T \lesssim 20$  K, the data suggest changes in the low energy electronic structure, likely due to short range antiferromagnetic correlations between local moments.

## II. EXPERIMENTAL DETAILS

Here, we study temperature and excitation density dependent carrier relaxation dynamics by tracking reflectivity changes of  $\text{YbB}_{12}$  single crystal using 60 femtosecond (fs) near-infrared optical pulses (800 nm) for both pump and probe. A disk-shaped sample, 4.5 mm in diameter, was cut from the single crystal [28] and mechanically polished for optical measurements [25]. Experiments were performed with a Ti:sapphire laser amplifier operating at 250 kHz, employing a double modulation fast-scan technique.

The reported measurements cover a range of excitation densities between  $0.5 \mu\text{J}/\text{cm}^2$  and  $0.5 \text{mJ}/\text{cm}^2$ . Thus, continuous laser heating effects should be considered. The average heating of the excited spot is mainly governed by the thermal conductivity of the sample and can be easily calculated using a simple steady-state heat diffusion model [33]. Thermal conductivity of  $\text{YbB}_{12}$  exceeds  $10 \text{W}/\text{mK}$  over the entire range of temperatures in question [34]. Taking into account the optical constants [25] and considering the worst case scenario (base temperature of 5 K and excitation density of  $410 \mu\text{J}/\text{cm}^2$ ), the average laser heating amounts to only 1.1 degrees in  $\text{YbB}_{12}$  and can thus be neglected.

## III. RESULTS

Figure 1 presents the raw data recorded as a function of (a) excitation density (at base temperature of 5 K) and (b) temperature (at a constant fluence,  $F = 8 \mu\text{J}/\text{cm}^2$ ). For  $F \lesssim 20 \mu\text{J}/\text{cm}^2$ , the excitation density dependence data display slightly sublinear dependence of amplitude on fluence, yet the characteristic timescales remain constant. For higher fluences, both amplitudes as well as the characteristic timescales show a strong dependence on  $F$ . To follow the  $T$  dependence of the dynamics in the low excitation limit we thus chose  $F = 8 \mu\text{J}/\text{cm}^2$  [Fig. 1(b)].

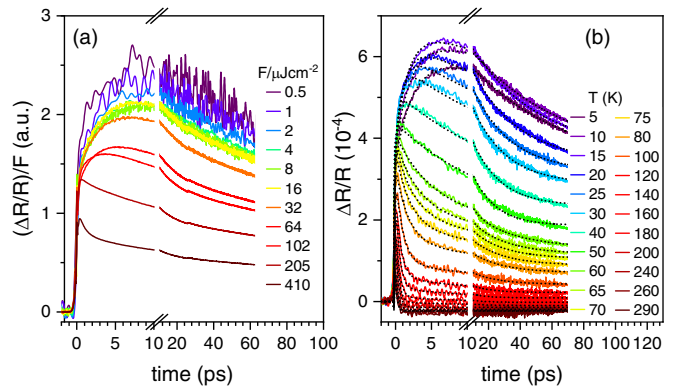


FIG. 1. Dynamics of photoinduced change in reflectivity of the  $\text{YbB}_{12}$  single crystal at 800 nm. (a) Dynamics recorded at 5 K base temperature as a function of  $F$  over three orders of magnitude. All traces were normalized to  $F$ . (b)  $T$  dependence of reflectivity traces recorded at  $F = 8 \mu\text{J}/\text{cm}^2$ . Dashed lines are fits to the data (see text). Note the break in the x axis. Continuous laser heating is less than 1 K over the entire range of temperatures and excitation densities.

### A. $T$ -dependent dynamics in the weak perturbation regime

We start by discussing the  $T$  dependence of dynamics in the low excitation regime. From Fig. 1(b) one can clearly see a strong  $T$  dependence of the recovery time, which varies between several tens of ps at 5 K to about 1 ps at 80 K. Moreover, the data at  $T \leq 40$  K display a slow picosecond buildup. While such was not observed in  $\text{SmB}_6$  [11], in superconductors it has been attributed to pair breaking by the absorption of high-frequency phonons, created during the relaxation of hot carriers towards the gap [21,22].

To quantify the  $T$  dependence of the amplitude and recovery time we first fit the photoinduced reflectivity traces with

$$\frac{\Delta R}{R}(t) = H(t)[A_1(1 - e^{-\frac{t}{\tau_{\text{rise}}}})e^{-\gamma t} + A_2]. \quad (1)$$

Here  $A_1$ ,  $\tau_{\text{rise}}$ , and  $\gamma$  are the amplitude, rise time, and the decay rate of the response,  $A_2$  accounts for a remaining bolometric signal at  $t \gg 100$  ps, and  $H(t)$  is the step function with a resolution limited rise time of  $\sim 100$  fs. This simple fit function accounts well the data at  $T < 60$  K; at higher  $T$  the entire recovery time window is better fit by a double exponential decay.

The overall slowing down of the relaxation upon cooling is an indication of an energy gap in the excitation spectrum. It has been observed both in superconductors [20–23] as well as in heavy electron systems [10–12,14,18], attributed to a boson (phonon) bottleneck [12,20]. Here, following photoexcitation, hot electrons and holes first relax via e-e and e-ph collisions towards the gap, resulting in excess densities of electrons-hole pairs (EHP) and high frequency ( $\hbar\omega > E_g$ ) phonons (HFP). We assume the electron-hole symmetry with densities of electrons and holes being the same ( $n$ ). The presence of the gap hinders the recombination of excess EHPs due to the competing creation of pairs by HFP absorption, resulting in a phonon bottleneck [20]. In this case, it is the slow decay of the HFP population (via anharmonic decay or via diffusion out of the

excitation volume) that governs the relaxation rate  $\gamma$  of the coupled EHP-HFP system back to equilibrium.

The time evolution of the system is given by a set of two coupled differential equations [20]:

$$\begin{aligned} \dot{n} &= \beta N - Rn^2 + n_0\delta(t) \\ \dot{N} &= -[\beta N - Rn^2]/2 - (N - N_0)\tau_\gamma^{-1} + N_0\delta(t). \end{aligned} \quad (2)$$

Here,  $n$  and  $N$  are the EHP and HFP densities, respectively,  $\beta$  is the probability of pair creation by HFP absorption, and  $R$  is the bare EHP recombination rate with the creation of HFP.  $\tau_\gamma^{-1}$  is the decay rate of HFP, governed, e.g., by anharmonicity, and can be approximated as being  $T$  independent. Note that the microscopic parameter  $\tau_\gamma$  differs from the measured recovery rate  $\gamma$ , the latter reflecting the recovery of the coupled EHP-HFP system [20]. Finally,  $n_0$  and  $N_0$  are the EHP and HFP densities created during the initial avalanche process (on a 100-fs timescale). These are determined from the absorbed energy density  $\Theta$ , considering an energy  $E_g$  per HFP and  $E_g/2$  per electron and hole, such that  $n_0 = \frac{2\Theta r}{E_g}$  and  $N_0 = \frac{\Theta(1-r)}{E_g}$ . Here  $0 \leq r \leq 1$  is the fraction of  $\Theta$  in the EHP channel and can be determined from the  $F$  dependence of the ps buildup, addressed in Sec. III B.

We now make use of the bottleneck model [11,20] for a quantitative analysis of the data to gain information on the  $T$  dependence of the low energy gap in YbB<sub>12</sub>. We analyze the  $T$  dependence of the amplitude of reflectivity transient and its relaxation rate (the  $T$  and  $F$  dependence of the ps buildup is addressed below). As  $\tau_\gamma$  is the largest timescale, the initial thermalization between EHPs and HFPs on the ps timescale results in a quasiequilibrium state, given by the detailed balance equation

$$Rn_s^2 = \beta N_s, \quad (3)$$

where  $n_s$  and  $N_s$  are the quasithermal concentrations of EHPs and HFPs at some new effective temperature  $T^*$  [35], see also Appendix. Assuming no energy is yet transferred to phonons with energy smaller than the gap, this quasistationary case is given by

$$Rn_s^2 = \beta N_s; n_s = \frac{\beta}{4R} [\sqrt{1 + 8R\beta^{-1}(2n_0 + N_0)} - 1]. \quad (4)$$

Once this quasiequilibrium state has been reached, the coupled system relaxes through the decay of HFPs.

In the weak perturbation limit, the amplitude or reflectivity change  $A_1$  is proportional to excess EHP density. At finite temperatures,  $A_1 \propto (n_s - n_T)$ , where  $n_T$  is the density of thermally excited EHPs. Taking into account the detailed balance equation, Eq. (4), it has been shown [11,17,18,20] that  $n_T(T)$  and thus  $E_g(T)$  can be extracted from the measured  $A_1(T)$  via [12,20]:

$$n_T(T) \propto A_1(0)A_1^{-1}(T) - 1. \quad (5)$$

Here  $A_1(0)$  is the amplitude in the limit when  $T \rightarrow 0$  K. With  $n_T(T) \propto N(0)(E_g T)^p e^{-E_g/2k_B T}$  [36], where  $N(0)$  is the normal state density of states and power  $p$  depends on the exact shape of the DOS,  $E_g(T)$  can be estimated.

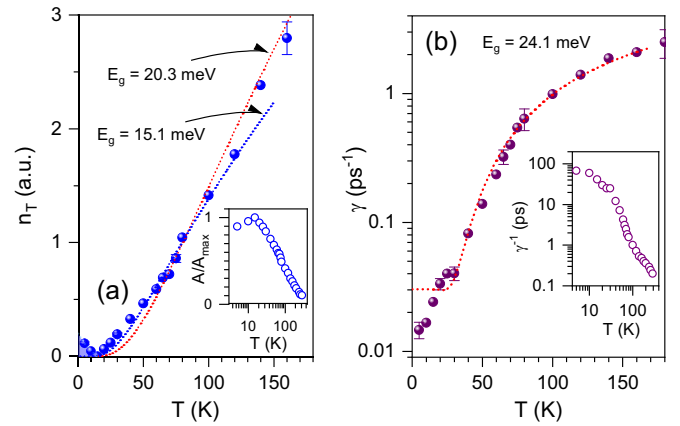


FIG. 2.  $T$  dependence of (a) thermally excited EHP density extracted from the  $T$  dependence of  $A_1$ , presented in the inset, and (b) the relaxation rate  $\gamma$ . The data were recorded at  $F = 8 \mu\text{J}/\text{cm}^2$ . The solid spheres are the experimental data and the dotted lines are fits to the data (see text).

The inset to Fig. 2(a) presents the  $T$  dependence of  $A_1$ , obtained by taking maximum values of reflectivity transients presented in Fig. 1(b). Upon cooling down,  $A_1$  displays continuous growth down to  $\approx 20$  K. Below 20 K, however,  $A_1$  does not saturate, but shows a decrease—similarly as in SmB<sub>6</sub> [18]. The main panel of Fig. 2(a) presents  $n_T(T)$ , extracted through Eq. (5), where the maximum amplitude was used as  $A_1(0)$ . Above 20 K, we fit the extracted  $n_T(T)$  using  $p = 1/2$ , which corresponds to the variation of the DOS near the gap edge, similar to a superconductor (the fit is rather insensitive to small variations in  $p$ ). The gradual increase of  $n_T$  with increasing  $T$  suggests that the hybridization gap is present to  $T > 200$  K. In the fit, we consider  $E_g$  to be  $T$  independent within the temperature range in question ( $T < 200$  K). We did consider different  $T$  dependences of  $E_g$ , similar to those extracted for Ce<sub>3</sub>Bi<sub>4</sub>Pt<sub>3</sub> [2,37], yet no major improvement in the fit quality can be achieved. The extracted values for  $E_g$ , shown in Fig. 2(a), are around 15 meV, consistent with earlier spectroscopic studies [24,28].

We note a decrease in amplitude below  $\approx 20$  K, reproduced by several measurements on different days. Since at these low temperatures  $n_T$  is always low compared to the density of photoexcited EHPs, a decrease in the signal is most likely caused by a (slight) increase in the gap energy scale or by sharpening of the peaks in the DOS, as suggested by recent tunneling data on SmB<sub>6</sub> [38].

In the low excitation limit the recovery rate  $\gamma$  has also been shown to be governed by  $n_T$  [12], where  $\gamma \propto [D(En_T + 1)^{-1} + 2n_T]$ , with  $D$  and  $E$  being the  $T$ -independent proportionality constants. Indeed, as shown in Fig. 2(b),  $\gamma$  is continuous to increase up to the highest  $T$ . Fitting the data, using the same functional form for  $n_T$ , we obtain a somewhat higher value for  $E_g = 24$  meV. Also here, a departure from the high temperature behavior is seen below  $\approx 20$  K, consistent with changes in the low energy structure. Given the simple approximations for the shape of the DOS and assuming the gap to be simply  $T$  independent, the overall agreement with the model is very good.

The observation of departure from constant gap behavior below 20 K implies changes in the low energy excitation spectrum at low  $T$ . Similar departure from the high- $T$  behavior was observed at low  $T$  also in  $\text{SmB}_6$  [18]. Together with the large residual THz conductivity, the observation in  $\text{SmB}_6$  was attributed to a (topological) surface state. In  $\text{YbB}_{12}$ , however, the residual THz optical conductivity is at least two orders of magnitude lower than in  $\text{SmB}_6$  [25], thus we exclude this possibility. Instead, we argue that correlations between local moments give rise to changes in the low energy excitation spectra. Indeed, inelastic neutron scattering data do provide evidence for short range antiferromagnetic fluctuations at comparable temperatures [39].

### B. Excitation density dependence at 5 K

The  $T$ -dependent study implies the hybridization to be present nearly up to room temperature, where the relaxation time becomes comparable to the e-ph thermalization in the metallic state. The question is: How robust is  $c$ - $f$  hybridization with respect to the electronic excitation? Moreover, the peculiar behavior of a finite  $T$ - and  $F$ -dependent rise time needs addressing. As shown in Fig. 1, the instantaneous buildup of photoexcited carrier density on a  $\sim 100$  fs timescale is followed by a further increase on a ps timescale. The delayed rise time gradually decreases with increasing excitation density and finally becomes resolution limited for  $F > 100 \mu\text{J}/\text{cm}^2$ .

In superconductors, the observation of the ps buildup has been attributed to Cooper pair breaking by reabsorption of HFPs, taking place during the formation of the quasistationary state between the condensate, broken pairs, and HFPs [21,22,40], see also Eq. (4). The nonlinear nature of this so-called pre-bottleneck dynamics [19,20] could be used to determine microscopic parameters, such as the e-ph coupling constant in NbN [22]. Moreover, as such nonlinear dynamics is limited to a range of excitation densities, for which the resulting gap suppression is perturbative only [22]; such a study provides the means to study the gaps robustness against electronic excitation.

For early time delays, where the HFP decay term can be neglected, Eq. (2) has analytic solutions for  $n(t)$  and  $N(t)$ , see Appendix and Ref. [20]. Moreover, densities of thermally excited EHPs and HFPs can also be neglected at low temperatures. The solutions thus depend only on the microscopic parameters  $R$ ,  $\beta$ , and the fraction of the absorbed energy density  $\Theta$  in the EHP channel  $0 \leq r \leq 1$ .  $\Theta$  is determined via  $\Theta = F(1 - \mathcal{R})/\lambda_{\text{opt}}$ , with the optical penetration depth  $\lambda_{\text{opt}} = 50$  nm and reflectivity  $\mathcal{R} = 0.3$  extracted from optical data [25].

We perform a global fit to the  $F$ -dependent data, with the excitation density  $F$  spanning over three orders of magnitude. We first determine the ( $F$ -dependent) values of the recovery rate  $\gamma$  by fitting the dynamics for  $t > 10$  ps by  $Be^{-\gamma t} + C$ . The resulting function is then multiplied by an analytic solution for pre-bottleneck kinetics, see Eq. (A1) in Appendix. Figure 3(a) presents the global fit of the data, using  $\gamma(F)$  shown in panel (c) and  $E_g = 15$  meV. An excellent agreement with the data is obtained, especially considering the large span of excitation densities. The extracted global param-

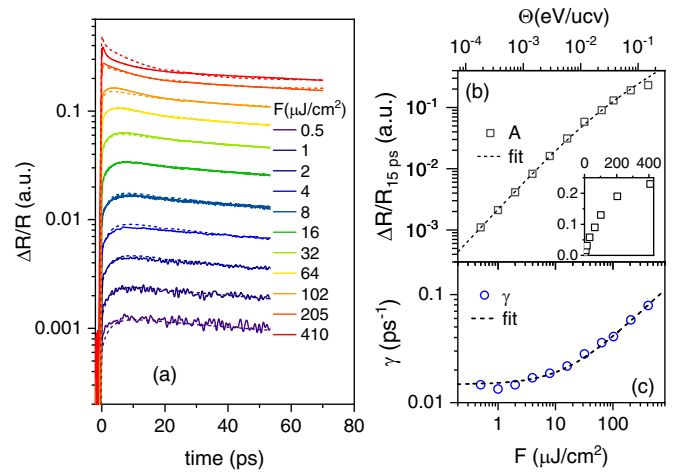


FIG. 3. The analysis of the  $F$  dependence of transient reflectivity at 5 K using the phonon-bottleneck model [20]. Panel (a) presents the data recorded for  $F$  spanning three orders of magnitude (solid lines) fit by the global fit (dashed lines), providing access to parameters  $R$ ,  $\beta$ , and  $r$ . (b) The  $F$  dependence of reflectivity change at 15 ps time delay (open black squares), together with the fit (dashed line) with  $n_s(F)$ , given by Eq. (4). Inset presents the same data on the linear scale. (c) The  $F$  dependence of the relaxation rate  $\gamma$  (open blue circles), fit by  $\gamma \propto (n_s + E)$  (dashed line). For all fits the same values of microscopic parameters were used:  $r = 0.47 + / - 0.01$ ,  $\beta = 0.61 + / - 0.01 \text{ ps}^{-1}$ , and  $R = 0.14 + / - 0.01 \text{ ps}^{-1} \text{ ucv}$ .

ters are:  $r = 0.47 + / - 0.01$ ,  $\beta = 0.61 + / - 0.01 \text{ ps}^{-1}$ , and  $R = 0.14 + / - 0.01 \text{ ps}^{-1} \text{ ucv}$ . Note a peculiar change in the character of the pre-bottleneck dynamics from being governed by pair generation (buildup) to being governed by the bimolecular recombination (decay) near  $100 \mu\text{J}/\text{cm}^2$ , see also simulation in Appendix. In superconductors such a change in dynamics has never been observed, since quenching of the gap takes place before this regime can be reached. The agreement between the data and the model thus implies no pronounced reduction of  $E_g$  up to  $F = 400 \mu\text{J}/\text{cm}^2$ , which corresponds to  $\Theta \approx 140$  meV per unit cell (i.e.,  $\sim 35$  meV per Yb). For comparison, this value exceeds values in superconductors with comparable gap sizes by two to three orders of magnitude [23].

Figure 3(b) presents the  $F$  dependence of  $\Delta R/R(15 \text{ ps})$ , where a quasistationary state, given by Eq. (4), is established. The best fit with Eq. (4) is shown by the dashed line, again in line with the model.

Finally, Fig. 3(c) presents  $\gamma(F)$ . For low temperatures,  $\gamma$  has been shown to follow  $\gamma \propto (n_s + n_T)$  [20]. Strictly speaking, this implies  $\gamma^{-1} \rightarrow \infty$  in the limit of  $T, F \rightarrow 0$ . However, the model does not take into account extrinsic effects, as for example the diffusion of hot carriers out of the probed volume [14]. Indeed, both  $T$ - and  $F$ -dependent data show a saturation of the relaxation time, i.e.,  $\gamma^{-1}(T, F \rightarrow 0) \approx 60$  ps, which is likely limited by the carrier transport into the bulk of the crystal. Taking this into account, we fit  $\gamma \propto (n_s + E)$ , with  $E$  being a constant, see dashed line in Fig. 3(c). The agreement with the model over a large range of excitations further evidences the robustness of hybridization against electronic excitation.

#### IV. DISCUSSION

Let us now turn to the extracted microscopic parameters. The ratio  $r \approx 0.5$  implies a high e-ph relaxation rate for hot carriers; a similar value is obtained in a conventional superconductor NbN [22]. The rate of the EHP creation by absorption of a phonon  $\beta$  is also similar to values obtained in NbN [22]. However, the extracted value of recombination rate  $R$  is in YbB<sub>12</sub> about three orders of magnitude lower than in NbN [22]. To address this, let us consider the detailed balance equation. From  $\eta/R = n_T^2/N_T$  it follows that the ratio  $\eta/R$  is governed by the (high temperature) densities of states of electrons and phonons.  $N_T$  can be estimated in the Debye approximation as  $N_T = 9\nu E_g^2 k_B T \omega_D^{-3} \exp(-E_g/k_B T)$ , where  $\nu$  is the number of atoms per unit cell and  $\omega_D$  is the Debye energy [20]. With  $n_T(T) \simeq N(0) \sqrt{\pi E_g k_B T} \exp(-E_g/2k_B T)$  it follows  $\eta/R = \frac{N(0)^2 \pi \omega_D^3}{9\nu E_g}$  [20]. Clearly, only a variation in  $N(0)$  can account for a 1000-fold increase of  $\eta/R$  in YbB<sub>12</sub> as compared to NbN. As the density of states of conduction band electrons are comparable for the two systems [41,42], this implies that hybridization not only results in the gap in the density of states but is accompanied by a pronounced charge transfer from the localized  $4f$  states into the hybridized band.

#### V. CONCLUSIONS

In summary, we show that in YbB<sub>12</sub> the hybridization gap persists to temperatures of the order of  $E_g/k_B$  and is extremely robust against electronic excitation. This is likely applicable to a larger class of Kondo lattice systems, as similar robustness can be inferred also from studies on SmB<sub>6</sub> [11] and heavy fermion systems [11,16]. A quantitative analysis of the density dependent carrier dynamics presented here provides access to microscopic parameters, revealing that hybridization is accompanied by a strong charge transfer from the localized  $4f$  levels. Finally, near 20 K, the relaxation dynamics in YbB<sub>12</sub> show a departure from the high- $T$  behavior, suggesting changes in the low-energy gap structure that can be attributed to short-range antiferromagnetic correlations between local moments.

#### ACKNOWLEDGMENTS

This project is funded by the Deutsche Forschungsgemeinschaft (DFG, German Research Foundation) TRR 173-268565370 (“Spin+X”, Project A05) and TRR 288-422213477 (“Elasto-Q-Mat”, Project B08).

#### APPENDIX: SIMULATIONS OF PRE-BOTTLENECK DYNAMICS

Considering  $\tau_\gamma$  being the largest timescale of the problem, the early timescale dynamics describes the buildup of the quasiequilibrium between the EHP and HFP subsystems, i.e., their densities reach a quasithermal equilibrium (the effective temperature, however, differs from the temperature of low frequency phonons). For this limiting case, exact analytical solutions for the time evolution of  $n$  and  $N$  have been derived for excitation densities where the resulting gap suppression is not too strong [20,21]. At low temperatures the density of thermally excited EHPs and HFPs can be neglected. Consid-

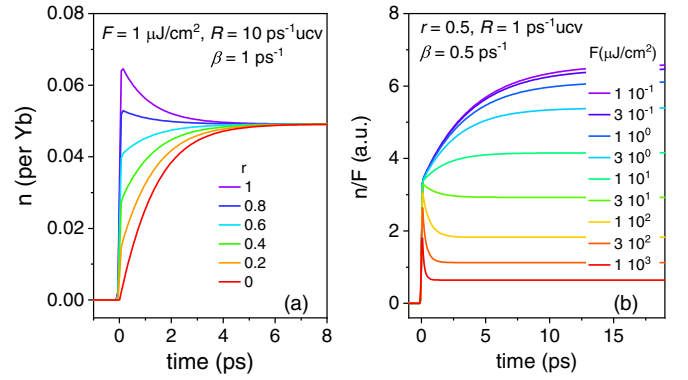


FIG. 4. Simulation of early stage QP dynamics in the absence of the decay channel (which proceeds via phonon escape/anharmonic decay). Panel (a) presents the evolution for constant  $F = 1$  mJ/cm<sup>2</sup> and different values of  $r$  from 1 (all the energy initially in the QP channel) to 0 (all the energy initially in the HFP channel). (b) Fluence dependence of dynamics for constant  $R$ ,  $b$ ,  $r$  (the values are given in the plot). Here  $n(t)$  is normalized to excitation fluence  $F$  to emphasize the nonlinearity of dynamics.

ering  $\tau_\gamma \rightarrow \infty$  and the initial conditions [ $n(t \approx 0) = n_0$  and  $N(t \approx 0) = N_0$ ], the coupled differential equations, Eq. (2), have the following analytical solution for  $n(t)$ :

$$n(t) = \frac{\beta}{R} \left[ -\frac{1}{4} - \frac{1}{2\tau} + \frac{1}{\tau(1 - Ke^{-t/\tau})} \right]. \quad (\text{A1})$$

Here,  $\tau^{-1}$  and  $K$  are the dimensionless parameters determined by the initial conditions  $n_0$ ,  $N_0$ , and the microscopic constants  $R$  and  $\beta$  [20,21]:

$$\tau^{-1} = \sqrt{\frac{1}{4} + \frac{2R}{\beta}(n_0 + 2N_0)}$$

$$K = \frac{\frac{\tau}{2} \left( \frac{4Rn_0}{\beta} + 1 \right) - 1}{\frac{\tau}{2} \left( \frac{4Rn_0}{\beta} + 1 \right) + 1}. \quad (\text{A2})$$

Figure 4 presents different limiting cases for  $n(t)$  in this pre-bottleneck regime, which depend on the microscopic parameters  $R$  and  $\beta$ , as well as on the initial conditions, which are given by the ratio  $r$  and absorbed energy density  $\Theta$  [23]. Here,  $n(t)$  is obtained by convoluting Eq. (2) with the Heaviside step function, whose rise time is chosen to be 100 fs, and reflects the time resolution of the experiment as well as the characteristic time for the initial e-e and e-ph processes.

In this simulation, we consider parameters relevant for YbB<sub>12</sub>, with  $E_g = 15$  meV and excitation densities comparable to those used in the experiment. From the optical conductivity data [25] at 1.55 eV we extract the values of the dielectric functions  $\epsilon_1 \approx -0.498$  and  $\epsilon_2 \approx 3.12$ , and determine the optical penetration depth to be  $\lambda_{\text{opt}} \approx 50$  nm. The absorbed energy density ( $\Theta$ ) is determined from the optical penetration depth and reflectivity at 1.55 eV of  $\mathcal{R} = 0.3$  as

$$\Theta = \frac{F(1 - \mathcal{R})}{\lambda_{\text{opt}}}.$$

As a reference, the incoming fluence  $F = 1$  mJ/cm<sup>2</sup> corresponds to  $\Theta = 364$  meV/ucv or 91 meV/Yb.

Figure 4(a) presents the simulation of the time evolution of the EHP density for constant excitation density  $\Theta$  but different values of  $r$ . Here,  $r = 1$  corresponds to the limit where all of the absorbed energy is initially in the EHP channel while  $r = 0$  corresponds to the other extreme case, where the entire energy is initially transferred to HFPs. For all values of  $r$  the same quasiequilibrium concentration of EHPs,  $n_s$ , is reached (determined simply by the detailed balance equation,  $Rn_s^2 = \beta N_s$ ). However, over a large range of values of parameter  $r$ , the initial excitation is followed by the generation of additional EHPs via HFP absorption, as manifested by the delayed buildup of  $n_s$  in Fig. 4(a).

Figure 4(b), on the other hand, presents the excitation density dependence of EHP dynamics using constant values of parameters  $R$ ,  $\beta$ , and  $r$ . It is reasonable to assume these parameters are in the first approximation independent of excitation density. The absorbed energy density  $\Theta$  (or  $F$ )

is varied here over four orders of magnitude. At the lowest fluences, the dynamics is obviously linear, governed solely by the electron-hole pair generation rate  $\beta$ . For higher excitation densities the dynamics becomes nonlinear, reflecting the bimolecular nature of electron-hole recombination. For fluence  $F$  between 10 and 100  $\mu\text{J}/\text{cm}^2$  (for the given choice of parameters) one indeed observes a change in the character of the pre-bottleneck dynamics, from being governed by the electron-hole-pair generation to being governed by the bimolecular recombination of EHPs.

In superconductors such a change in character of the dynamics has never been observed at high excitation densities. Most likely this can be attributed to the fact that the gap gets fully suppressed before such a regime can be reached. Our data on  $\text{YbB}_{12}$ , however, do display such a transition, underscoring the fact that the hybridization gap is extremely robust against electronic excitation.

- 
- [1] G. R. Stewart, *Rev. Mod. Phys.* **56**, 755 (1984).  
 [2] P. S. Riseborough, *Adv. Phys.* **49**, 257 (2000).  
 [3] L. Degiorgi, *Rev. Mod. Phys.* **71**, 687 (1999).  
 [4] P. Coleman, Heavy Fermions: Electrons at the Edge of Magnetism, in *Handbook of Magnetism and Advanced Magnetic Materials*, edited by H. Kronmüller, S. Parkin, M. Fähnle, S. Maekawa, and I. Zutic (John Wiley & Sons Inc., New York, 2007).  
 [5] A. C. Hewson, *The Kondo Problem to Heavy Fermions*, *Cambridge Studies in Magnetism* (Cambridge University Press, Cambridge, 1993).  
 [6] H. C. Choi, B. I. Min, J. H. Shim, K. Haule, and G. Kotliar, *Phys. Rev. Lett.* **108**, 016402 (2012).  
 [7] M. Guettler, A. Generalov, S. I. Fujimori, K. Kummer, A. Chikina, S. Seiro, S. Danzenbächer, Yu. M. Koroteev, E. V. Chulkov, M. Radovic, M. Shi, N. C. Plumb, C. Laubschat, J. W. Allen, C. Krellner, C. Geibel, and D. V. Vyalikh, *Nat. Commun.* **10**, 796 (2019).  
 [8] S. Ernst, S. Kirchner, C. Krellner, C. Geibel, G. Zwicky, F. Steglich, and S. Wirth, *Nature (London)* **474**, 362 (2011).  
 [9] S. Y. Agustsson, S. V. Chernov, K. Medjanik, S. Babenkov, O. Fedchenko, D. Vasilyev, C. Schlueter, A. Gloskovskii, Yu. Matveyev, K. Kliemt, C. Krellner, J. Demsar, G. Schönhense, and H. J. Elmers, *J. Phys.: Condens. Matter* (2021).  
 [10] J. Demsar, R. D. Averitt, K. H. Ahn, M. J. Graf, S. A. Trugman, V. V. Kabanov, J. L. Sarrao, and A. J. Taylor, *Phys. Rev. Lett.* **91**, 027401 (2003).  
 [11] J. Demsar, V. K. Thorsmølle, J. L. Sarrao, and A. J. Taylor, *Phys. Rev. Lett.* **96**, 037401 (2006).  
 [12] J. Demsar, J. L. Sarrao, and A. J. Taylor, *J. Phys.: Condens. Matter* **18**, R281 (2006).  
 [13] K. S. Burch, E. E. M. Chia, D. Talbayev, B. C. Sales, D. Mandrus, A. J. Taylor, and R. D. Averitt, *Phys. Rev. Lett.* **100**, 026409 (2008).  
 [14] J. Demsar, V. V. Kabanov, A. S. Alexandrov, H. J. Lee, E. D. Bauer, J. L. Sarrao, and A. J. Taylor, *Phys. Rev. B* **80**, 085121 (2009).  
 [15] E. E. M. Chia, J.-X. Zhu, D. Talbayev, H. J. Lee, N. Hur, N. O. Moreno, R. D. Averitt, J. L. Sarrao, and A. J. Taylor, *Phys. Rev. B* **84**, 174412 (2011).  
 [16] D. Leuenberger, J. A. Sobota, S.-L. Yang, H. Pfau, D.-J. Kim, S.-K. Mo, Z. Fisk, P. S. Kirchmann, and Z.-X. Shen, *Phys. Rev. B* **97**, 165108 (2018).  
 [17] Y. P. Liu, Y. J. Zhang, J. J. Dong, H. Lee, Z. X. Wei, W. L. Zhang, C. Y. Chen, H. Q. Yuan, Y. F. Yang, and J. Qi, *Phys. Rev. Lett.* **124**, 057404 (2020).  
 [18] J. Zhang, J. Yong, I. Takeuchi, R. L. Greene, and R. D. Averitt, *Phys. Rev. B* **97**, 155119 (2018).  
 [19] A. Rothwarf and B. N. Taylor, *Phys. Rev. Lett.* **19**, 27 (1967).  
 [20] V. V. Kabanov, J. Demsar, and D. Mihailovic, *Phys. Rev. Lett.* **95**, 147002 (2005).  
 [21] J. Demsar, R. D. Averitt, A. J. Taylor, V. V. Kabanov, W. N. Kang, H. J. Kim, E. M. Choi, and S. I. Lee, *Phys. Rev. Lett.* **91**, 267002 (2003).  
 [22] M. Beck, M. Klammer, S. Lang, P. Leiderer, V. V. Kabanov, G. N. Gol'tsman, and J. Demsar, *Phys. Rev. Lett.* **107**, 177007 (2011).  
 [23] J. Demsar, *J. Low Temp. Phys.* **201**, 676 (2020).  
 [24] M. Okawa, Y. Ishida, M. Takahashi, T. Shimada, F. Iga, T. Takabatake, T. Saitoh, and S. Shin, *Phys. Rev. B* **92**, 161108(R) (2015).  
 [25] H. Okamura, T. Michizawa, T. Nanba, S. ichi Kimura, F. Iga, and T. Takabatake, *J. Phys. Soc. Jpn.* **74**, 1954 (2005).  
 [26] Y. Takeda, M. Arita, M. Higashiguchi, K. Shimada, H. Namatame, M. Taniguchi, F. Iga, and T. Takabatake, *Phys. Rev. B* **73**, 033202 (2006).  
 [27] K. Hagiwara, Y. Ohtsubo, M. Matsunami, S. Ideta, K. Tanaka, H. Miyazaki, J. E. Rault, P. Le Fèvre, F. Bertran, A. Taleb-Ibrahimi *et al.*, *Nat. Commun.* **7**, 12690 (2016).  
 [28] F. Iga, N. Shimizu, and T. Takabatake, *J. Magn. Magn. Mater.* **177-181**, 337 (1998).  
 [29] Z. Xiang, Y. Kasahara, T. Asaba, B. Lawson, C. Tinsman, L. Chen, K. Sugimoto, S. Kawaguchi, Y. Sato, G. Li *et al.*, *Science* **362**, 65 (2018).  
 [30] Y. Xu, S. Cui, J. K. Dong, D. Zhao, T. Wu, X. H. Chen, K. Sun, H. Yao, and S. Y. Li, *Phys. Rev. Lett.* **116**, 246403 (2016).  
 [31] O. Erten, P.-Y. Chang, P. Coleman, and A. M. Tsvetlik, *Phys. Rev. Lett.* **119**, 057603 (2017).

- [32] R. Peters, T. Yoshida, and N. Kawakami, *Phys. Rev. B* **100**, 085124 (2019).
- [33] D. Mihailovic and J. Demsar, *Spectroscopy of Superconducting Materials*, ACS Symposium Series **730**, 230 (1999).
- [34] F. Iga, T. Suemitsu, S. Hiura, K. Takagi, K. Umeo, M. Sera, and T. Takabatake, *J. Magn. Magn. Mater.* **226-230**, 137 (2001).
- [35] W. H. Parker, *Phys. Rev. B* **12**, 3667 (1975).
- [36] V. V. Kabanov, J. Demsar, B. Podobnik, and D. Mihailovic, *Phys. Rev. B* **59**, 1497 (1999).
- [37] B. Bucher, Z. Schlesinger, P. Canfield, and Z. Fisk, *Phys. B: Condens. Matter* **199-200**, 489 (1994).
- [38] X. Zhang, N. P. Butch, P. Syers, S. Ziemak, R. L. Greene, and J. Paglione, *Phys. Rev. X* **3**, 011011 (2013).
- [39] J.-M. Mignot, P. A. Alekseev, K. S. Nemkovski, L.-P. Regnault, F. Iga, and T. Takabatake, *Phys. Rev. Lett.* **94**, 247204 (2005).
- [40] M. Beck, M. Klammer, I. Rousseau, M. Obergfell, P. Leiderer, M. Helm, V. V. Kabanov, I. Diamant, A. Rabinowicz, Y. Dagan, and J. Demsar, *Phys. Rev. B* **95**, 085106 (2017).
- [41] D. J. Chadi and M. L. Cohen, *Phys. Rev. B* **10**, 496 (1974).
- [42] M. Heinecke, K. Winzer, J. Noffke, H. Kranefeld, H. Grieb, K. Flachbart, Y. B. Paderno, *Z. Phys. B* **98**, 231 (1995).